JOURNAL OF VIROLOGY, Aug. 1988, p. 2701–2711
0022-538X/88/082701-11$02.00/0

Vol. 62, No. 8

Role of Cytoplasmic Vacuoles in Varicella-Zoster Virus Glycoprotein Trafficking and Virion Envelopment

FRANK JONES AND CHARLES GROSE*

Departments of Microbiology and Pediatrics, University of Iowa College of Medicine, Iowa City, Iowa 52242

Received 8 February 1988/Accepted 29 April 1988

Varicella-zoster virus (VZV) encodes several glycoproteins which are present on both mature viral envelopes and the surfaces of infected cell membranes. Mechanisms of VZV glycoprotein transport and virion envelopment were investigated by both continuous radiolabeling and pulse-chase analyses with tritiated fucose in VZV-infected cells. We studied in detail the large cytoplasmic vacuoles which were present in infected cells but absent from uninfected cells. The specific activity in each subcellular compartment was defined by quantitative electron microscope autoradiography, using a cross-fire probability matrix analysis to more accurately assess the individual compartment demarcated by the silver grains. By these techniques, we documented a progression of activity originating in the Golgi apparatus and traveling through the post-Golgi region into virus-induced cytoplasmic vacuoles and finally to areas of the cellular membrane associated with the egress of viral particles. Significant amounts of radiolabel were not observed in the nucleus, and only low levels of radiolabel were associated with the cellular membrane not involved with the egress of viral particles. In addition, immunolabeling of Lowicryl-embedded VZV-infected cells demonstrated the presence of VZV glycoproteins within cytoplasmic vacuole membranes as well as on virion envelopes. These observations suggested that cytoplasmic vacuoles harbored VZV-specified glycoproteins and were also the predominant site of VZV virion envelopment within the infected cell. Neither enveloped nor unenveloped viral particles were observed within the Golgi apparatus itself.

Varicella-zoster virus (VZV) is a member of the herpesvirus family, members of which are characterized by a linear double-stranded DNA genome enclosed within an icosahedral capsid. VZV nucleocapsids are in turn covered by a lipid-rich envelope containing several virus-specified glycoproteins (reviewed in reference 11). After adsorption at the cellular membrane and penetration of uncoated virions, the first stage of viral replication takes place within the nucleus. Viral DNA packaging into capsids also occurs within the nucleus, after which an unstable and poorly defined region termed the tegument becomes attached to the nucleocapsid. Envelopment of the prototypic herpes simplex virus (HSV) is usually considered to occur at the inner nuclear membrane (8, 26, 27, 29, 32, 39); however, the de novo formation of an envelope around nucleocapsids within the nucleus has also been reported (2, 13).

The egress of mature VZV virions from infected cells may occur by two processes. Enveloped virions may migrate to the cellular membrane by cytoplasmic streaming (19, 27), or virions transported to the cellular membrane within cytoplasmic vacuoles may be released by reverse phagocytosis (19, 27). Large cytoplasmic vacuoles have also been observed in VZV-infected cells (7, 12, 25); equally importantly, previous work in this laboratory failed to show similar cytoplasmic vacuoles in uninfected cells. These differences suggested that the glycoprotein-laden vacuoles may be involved in the envelopment and egress of VZV from infected cells (25). In this communication the origin, glycoprotein composition, and possible role of cytoplasmic vacuoles in VZV envelopment were investigated by both continuous and pulse-chase radiolabeling experiments in VZV-infected cells. Using a cross-fire probability matrix (CFPM) analysis (4), we calculated the relative specific radioactivity within each subcellular compartment. On the basis of these data we propose a model of VZV envelopment.

MATERIALS AND METHODS

Cells and virus. The cell substrate was the Mewo strain of human melanoma cells (HMC; 12). Monolayer cultures were grown in Eagle minimum essential medium supplemented with 10% fetal bovine serum–2 mM glutamine–1.0% nonessential amino acids–penicillin (100 U/ml)–streptomycin (100 μg/ml; MEM-FBS). Stock virus for all experiments was the VZV 32 strain (10), which has been passed <20 times in culture.

Isotopic labeling of VZV-infected cells. HMC monolayers cultured in petri dishes (60 by 15 mm) were inoculated with trypsin-dispersed VZV-infected cells at an uninfected-to-infected cell ratio of six and incubated at 32°C with humidified 5.0% CO_2 in air. After 18 h, the MEM-FBS was replaced with fresh medium containing 30 μCi of L-[5,6-^{3}H]fucose (specific activity, 48.4 Ci/mmol) for continuous labeling experiments or with 115 μCi of L-[5,6-^{3}H]fucose (specific activity, 60.0 Ci/mmol) for pulse-chase labeling experiments. The continuously labeled cultures were incubated at 32°C for 2 or 24 h, after which time the monolayers were harvested and processed for electron microscopy. For pulse-chase labeling experiments the monolayers were incubated with [^{3}H]fucose for 30 min. The medium containing radioisotope was subsequently replaced with fresh MEM-FBS, and the monolayers were incubated at 32°C for additional times before processing for electron microscopy.

Fixation of labeled monolayers for light and electron microscope autoradiography. Radiolabeled monolayers were washed extensively with 10 mM phosphate-buffered saline (PBS) (pH 7.4) and fixed in situ with freshly prepared Karnovsky's fixative (17) for 30 min at ambient temperature. After three washes in 0.1 M sodium cacodylate (pH 7.2) containing 7% sucrose, the monolayers were postfixed in

* Corresponding author.

reduced osmium (1% $0sO_4$ and 1.5% potassium ferrocyanide in 0.1 M sodium cacodylate [pH 7.2]; 18). The cells were rinsed in dionized-distilled H_2O and dehydrated with a graded ethanol series. The monolayers were lifted from the petri dishes with propylene oxide and embedded in Spurr's resin (Polysciences, Warrington, Penn.) at 70°C overnight.

Light microscope autoradiography. Light microscope autoradiographs (ARGs) were prepared by drying xylene-expanded thick sections (0.5 μm) onto gelatin-coated slides (35). The slides were dipped into a 1:1 dilution of nuclear emulsion (NTB2; Eastman Kodak Co., Rochester, N.Y.) at 45°C and dried horizontally at 20 to 22°C. The emulsion-coated slides were stored in light-tight boxes with desiccator capsules (Dricap; Ted Pella, Tustin, Calif.) at 4°C. Silver grains were developed after 1 to 16 days in a 1:1 dilution of freshly prepared D19b (20) at 20°C for 6.5 to 7.0 min. The sections were stained with 0.5% toluidine blue in 0.5% sodium borate on a hot plate at 38 to 40°C. The stained tissue was differentiated with 50% ethanol for 30 to 60 s.

Electron microscope autoradiography. Tissue blocks for the electron microscope autoradiographic analysis were selected based on morphological preservation and grain distribution observed in the light microscope ARGs. Chloroform-expanded thin sections (120 nm, pale-gold interface color) were transferred to Formvar (1% Formvar solution in ethylene dichloride)-coated 200-mesh nickel grids. The sections were stained with 5% uranyl acetate for 30 min and with Reynolds lead citrate (33) for 15 min. A thin layer of evaporated carbon (light-tan deposit) was applied to the grids, and they were mounted onto small corks with perforated double-stick tape. A monocrystalline layer of gelled Ilford L4 nuclear emulsion (Polysciences) was applied to mounted grids by standard looping techniques (47). The grids were stored with Dricap desiccator capsules and were exposed at 4°C for 1 to 7 weeks. Silver grain development was with freshly prepared D19b for 2.0 to 2.5 min at 20°C. Unlabeled sections were also processed as described above for positive and negative chemography controls.

Quantitative analysis of the ARG by CFPM. Each electron microscope ARG was viewed with a Hitachi H-7000 electron microscope. Random micrograph fields were taken at a magnification of ×7,000, and each micrograph was printed at a final true magnification of ×18,750. Quantitative analysis of the micrographs was performed by using a simplified form of the CFPM and others described by Blackett and Parry (4, 9, 49). (The cross-fire correction program used for our CFPM analysis was prepared by P. Armstrong and M. A. Williams, University of Sheffield, and was adapted for the IBM computer by M. M. Friedman and A. Friedman, Georgetown University.) Briefly, the material was divided into mutually exclusive subcellular compartments; the radioactivity was assumed to be uniformly distributed within each compartment. A cross-fire correction overlay screen consisting of a regular array of point sources, each with six associated hypothetical disintegration points, was placed over the micrograph to be analyzed. (For an example of the cross-fire correction overlay screen, see Fig. 4). The subcellular compartment underlying each point source together with the subcellular compartment underlying each hypothetical disintegration was recorded in the CFPM. Each row of the CFPM represented the point source position, and each column represented the hypothetical disintegration position. Thin point sources, such as membranes, were expanded by placing the diameter of a circle over the membrane (46). Therefore, any points or silver grains within these expanded areas were recorded as originating from within the membrane. A reasonable circle diameter of 9.0 mm was used, which at a magnification of ×18,750 is defined to include 50% of the disintegrations originating from a thin-line source (38). In addition, all points and silver grains within 0.5 μm (9.5 mm at a magnification of ×18,750) of the trans-Golgi cisternae were recorded as originating from within the post-Golgi region. Finally, the positions of real silver grains were recorded as the subcellular compartment underlying the grain center (midpoint of the longest axis).

Each micrograph was analyzed in the manner described above, and the results for each time point were accumulated until 200 to 300 real grains had been recorded. Accumulative data within each row of the CFPM were normalized, and the cross-fire-corrected radioactive disintegrations for each subcellular compartment were calculated by using a version of Gaussian elimination on an IBM XT desk-top computer. The validity of the proposed model (radioactivity of each selected subcellular compartment must be uniformly distributed) was tested by further subdividing the subcellular compartments, collecting additional CFPM data, and determining whether the original model could accurately predict the radioactive disintegration distribution by χ^2 analysis. Once the model proved to be an accurate and unbiased representation of the tissue, the relative specific activity of each subcellular compartment was calculated by dividing the number of radioactive disintegrations by the relative area, obtained by standard stereological methods. These data were normalized so that a relative specific activity >1 represented significant radioactivity within the subcellular compartment.

Lowicryl K4M embedment of tissue. VZV-infected HMC monolayers were washed three times with PBS and fixed in situ with freshly prepared 5% paraformaldehyde in 0.1 M sodium cacodylate (pH 7.2) for 30 min at ambient temperature. The fixed monolayers were washed three times with 0.1 M sodium cacodylate (pH 7.2) and gently removed from the petri dish with a rubber cell scraper. The cell suspension was dehydrated with a graded dimethylformamide (DMF) series at −10°C and infiltrated with 1:2 Lowicryl K4M (Polysciences)-DMF (1 h), 1:1 Lowicryl K4M-DMF (1 h), 100% Lowicryl K4M (1 h), and 100% Lowicryl K4M (30 min) at −10°C (36). Polymerization was achieved by indirect UV irradiation at a sample-lamp distance of 8 cm for 16 h at 4°C. Thin sections (90 nm, silver-gold interface color) from polymerized blocks were cut with a glass knife, using a reduced water level, and were collected on 300-mesh nickel grids. The sections were stained with 5% uranyl acetate for 4 min and with Reynolds lead citrate for 3 min, or the sections were processed for immunocytochemistry.

Immunocytochemical procedure. Immunocytochemical localization of VZV gpI was performed on Lowicryl K4M-embedded tissue, using an indirect immunodetection system. Grids with thin sections were floated onto drops of PBS containing 1% bovine serum albumin for 10 min and were transferred to drops of anti-gpI monoclonal antibody (monoclone 3B3; 24, 45) diluted 1:20 in PBS for 1 h. The sections were washed for 30 min by floating the grids onto six successive drops of PBS, and then they were transferred to drops of goat anti-mouse immunoglobulin G conjugated with 10 nm gold (Janssen, Belgium) diluted 1:10 in PBS for 1 h. Immunostained sections were washed as described above, rinsed in deionized-distilled H_2O, and counterstained with 5% uranyl acetate for 4 min and with Reynolds lead citrate for 3 min. Specimens were viewed on a Hitachi H-600 electron microscope.

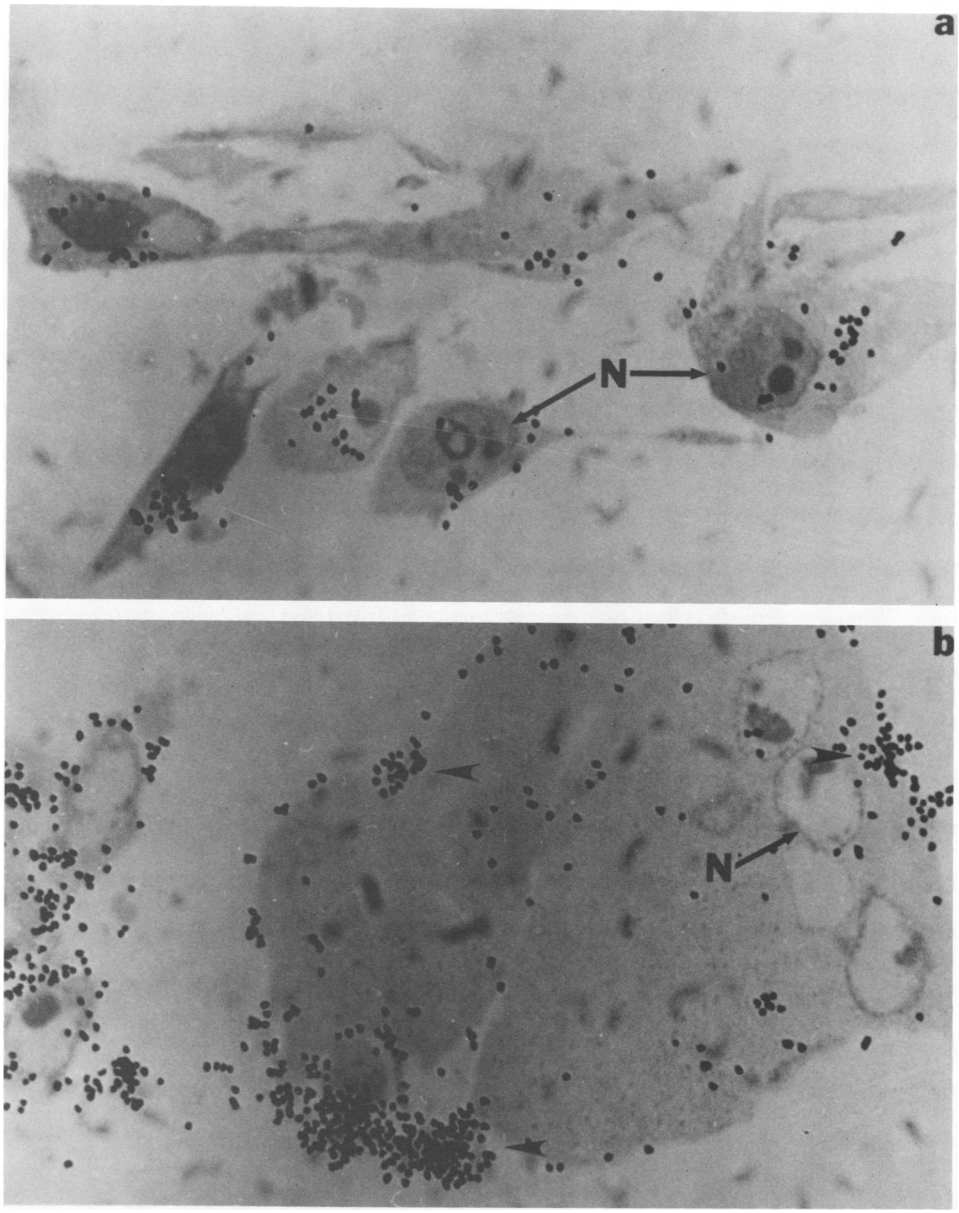

FIG. 1. Light microscope ARG of VZV-infected cells. Infected HMC monolayers were radiolabeled with [^{3}H]fucose for 2 (a) or 24 h (b) and processed for light microscope autoradiography as described in the text. After a 2-h radiolabeling period, [^{3}H]fucose was observed within the cytoplasm and accumulated at juxtanuclear regions. In contrast, after a 24-h radiolabeling period, silver grains accumulated at localized regions of the cellular membrane (arrowheads). These membrane regions may be involved with viral egress from infected cells. Abbreviation: N, nuclei. Magnification, ×1,200.

RESULTS

Localization of [^{3}H]fucose in ARGs by light microscopy. At the light microscopic level, characteristic silver grain distribution patterns could be recognized in VZV-infected monolayers. After a continuous 2-h labeling period with [^{3}H]fucose, silver grains were concentrated in juxtanuclear regions and to a lesser extent within the cellular membrane and cytoplasm (Fig. 1a). After a 24-h continuous labeling period with [^{3}H]fucose, we observed a large accumulation of silver grains within localized regions of the cellular membrane, probably associated with the egress of mature enveloped virions. Silver grains were also distributed within the cytoplasm and juxtanuclear regions (Fig. 1b). Uninfected cells continuously labeled for 2 h also accumulated grains in juxtanuclear regions and to a lesser extent within the cellular membrane and cytoplasm. However, after a 24-h continuous labeling period, silver grains were uniformly distributed within the cellular membrane and cytoplasm. Localized regions of silver grain accumulation at the cellular membrane, as described within VZV-infected cells, were not observed within uninfected cells (data not shown).

Localization of [^{3}H]fucose in ARGs by electron microscopy after continuous labeling. Figure 2 illustrates the distribution of [^{3}H]fucose activity in VZV-infected cells after a 24-h continuous labeling period. The accumulation of silver grains was clearly demonstrated within the Golgi apparatus,

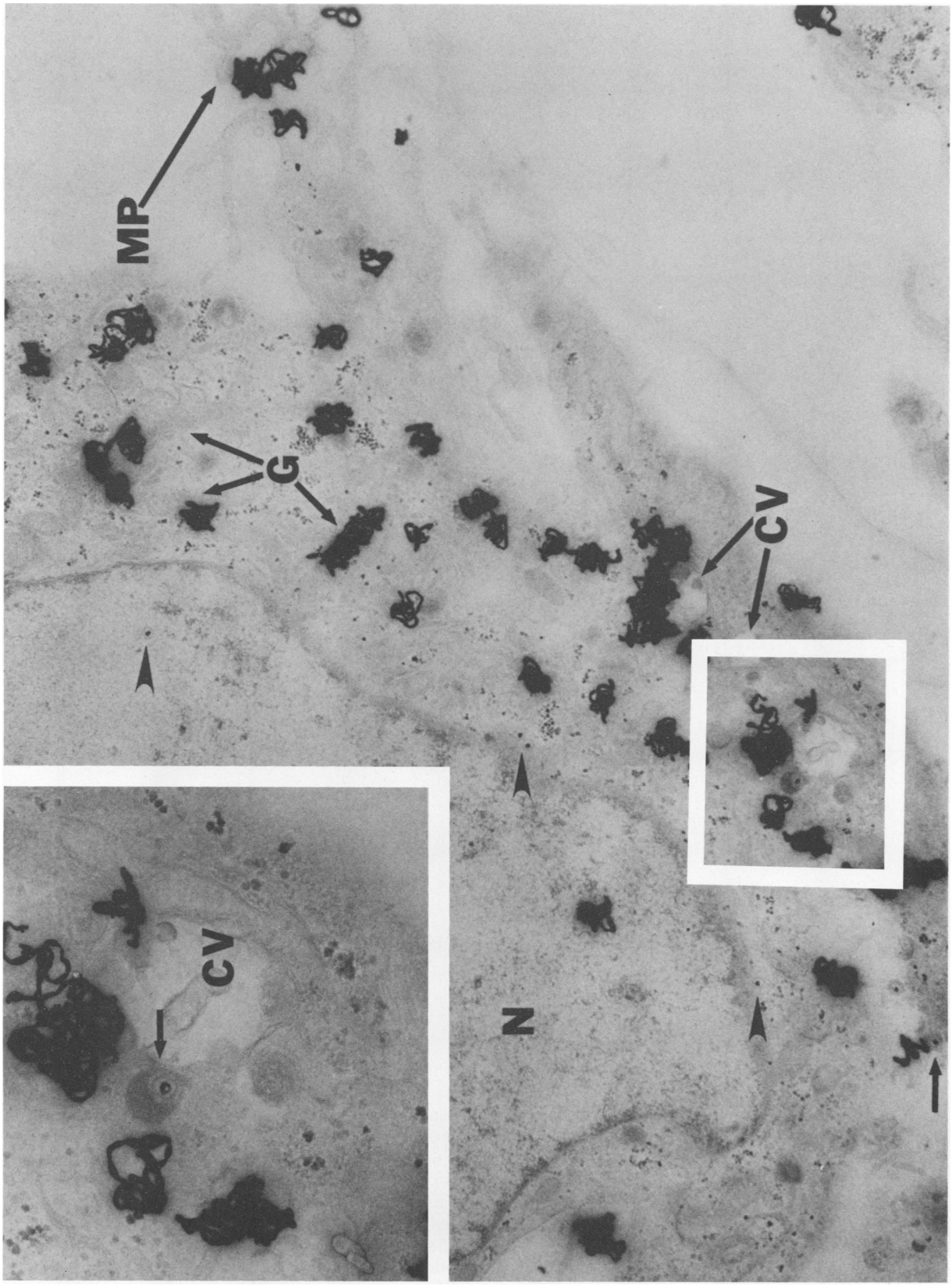

FIG. 2. Subcellular localization of viral glycoproteins within VZV-infected cells. Monolayers were radiolabeled with [^{3}H]fucose for 24 h beginning 12 h postinfection and were processed for electron microscope autoradiography as described in the text. Quantitation of silver grain distribution (Table 1) indicated a significant relative specific activity within the Golgi apparatus (G) and post-Golgi region, cellular membrane, and cytoplasmic vacuoles (CV). Naked nucleocapsids (arrowheads) were observed within the nucleus (N) and cytoplasm, whereas enveloped virions (arrows) were detected within cytoplasmic vacuoles (inset) and at the cellular membrane. Abbreviations: MP, microvillus projections. Magnification, ×16,770; inset, ×40,420.

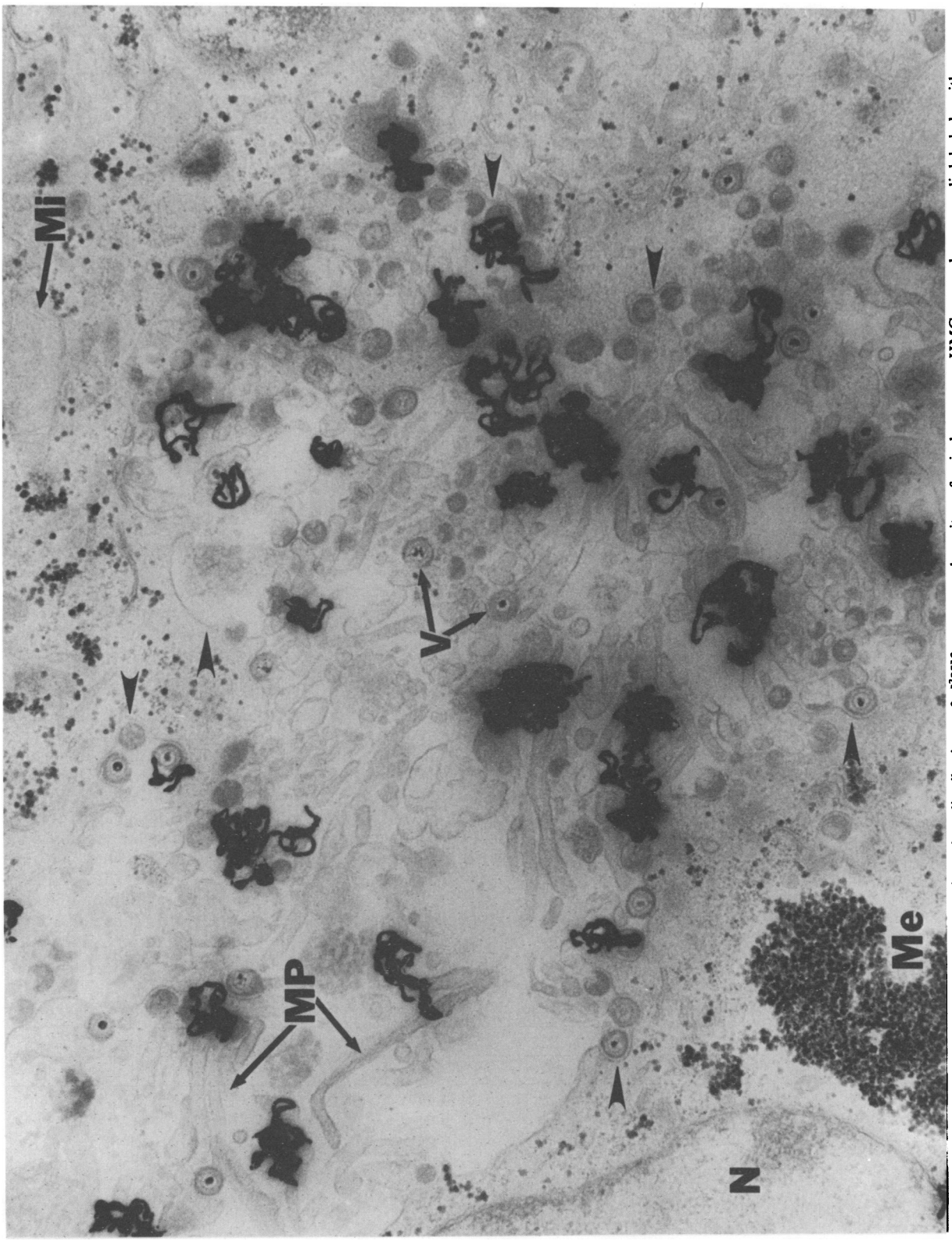

FIG. 3. VZV-infected cell illustrating the distribution of [^{3}H]fucose at the site of viral egress. HMC monolayers radiolabeled with [^{3}H]fucose for 24 h beginning 12 h postinfection were processed for electron microscope autoradiography as described in the text. Cytoplasmic vacuoles harboring enveloped virions migrated to localized regions of the cellular membrane in which fusion with the cellular membrane occurred, with a concomitant release of enveloped virions (V). Cytoplasmic vacuoles and cellular membrane fusion are clearly demonstrated in this figure (arrowheads). Abbreviations: Me, melanosome; Mi, mitochondria; MP, microvillus projections; N, nucleus. Magnification, ×32,680.

TABLE 1. Cross-fire analysis of silver grain distribution in VZV-infected cells continuously labeled with [^{3}H]fucose for 2 or 24 h

Subcellular compartment	Actual grains	Area	Disintegrations[a]	Relative sp act[b]
Cell membrane	30/16[c]	275/119	39/16	1.86/1.23
Cell membrane with virions[d]	0/44	0/47	0/76	0.00/14.77
Cytoplasm	43/54	488/746	16/16	0.43/0.19
Golgi bodies	15/24	9/27	43/36	62.42/12.25
Post-Golgi region	31/38	48/106	12/35	3.28/3.05
Cytoplasmic vacuoles	24/57	28/69	39/65	18.19/8.64
Nucleus	8/6	343/320	8/5	0.31/0.13
Extracellular space	10/11	927/848	4/0	0.05/−0.01

[a] Disintegrations were calculated by using the CFPM analysis of Blackett and Parry (4).

[b] Each relative specific activity value was calculated and normalized on an IBM XT desk-top computer so that subcellular compartments with significant radioactivities had values >1.

[c] Values to the left and right of the shill represent 2- and 24-h continuous labeling periods, respectively.

[d] Includes only cellular membrane areas associated with the egress of virions.

cytoplasmic vacuoles, and to a lesser extent within the post-Golgi region and cellular membrane. The cytoplasmic vacuoles appeared to be labeled primarily on their outer membranes and contained several enveloped virions. The prominent vacuoles ranged in diameter from 400 nm to 3.5 μm, with an average diameter of 900 nm. A typical localized region of viral egress at the cellular membrane is illustrated in Fig. 3. These regions were characterized by a large number of microvillus projections, cytoplasmic vacuoles, enveloped virions, and silver grains. The cytoplasmic vacuoles appeared to bud onto and thus expand the cellular membrane. This event resulted in the concomitant release of enveloped virions from the vacuoles and exposure of the glycoprotein-laden vacuole membrane at the cell surface. It should be noted that virions, enveloped or naked, were never observed within the Golgi apparatus itself, and enveloped virions associated with the nuclear membrane were only rarely observed.

A similar silver grain distribution was found within uninfected cells after a 24-h continuous [^{3}H]fucose labeling period. Silver grains were observed within the Golgi apparatus and the cellular membrane. However, labeling of uninfected cells did not lead to localized accumulation of silver grains within the cellular membrane. In addition, the large cytoplasmic vacuoles described above were never observed within uninfected cells.

Subcellular localization of viral glycoproteins as determined by quantitative analysis after continuous radiolabeling. To determine the subcellular localization of [^{3}H]fucose at both intermediate and late stages of VZV infection, infected monolayers were continuously labeled with [^{3}H]fucose and analyzed by quantitative electron microscope autoradiography with CFPM. The results are tabulated in Table 1. After a 2-h labeling period, significant levels of label (relative specific activity, >1) were obtained within the cellular membrane, Golgi apparatus, post-Golgi region, and cytoplasmic vacuoles. The greatest level of relative specific activity was reported within the Golgi apparatus and cytoplasmic vacuoles, whereas the cellular membrane and post-Golgi region only accumulated low levels of label. Insignificant levels of label (relative specific activity, <1) were reported within the cellular membrane associated with the egress of virions, cytoplasm, nucleus, and extracellular space. After a 24-h labeling period, the silver grain distribution should indicate each site of subcellular [^{3}H]fucose incorporation during the infection cycle (Fig. 2). As with the shorter labeling period, significant levels of radiolabel were seen within the cellular membrane, Golgi apparatus, post-Golgi region, and cytoplasmic vacuoles. However, by 24 h the greatest relative specific activity was found within the cellular membrane associated with the egress of virions (Fig. 3). Once again, insignificant levels of label were reported within the cytoplasm, nucleus, and extracellular space (Table 1).

Additional data included within Table 1 illustrate the importance of area and disintegration calculations when determining subcellular label incorporation in ARGs. When previous investigators expressed their results simply as the actual grains overlying a particular subcellular compartment, they did not take into account the relative area occupied by each subcellular compartment and the effect of cross-fire on their data analysis (32). This oversight will result in a misinterpretation of electron microscope autoradiographic data (9). For example, the actual number of grains observed after a 2-h continuous pulse within the cytoplasm was nearly three times greater than that observed within the Golgi apparatus (Table 1). However, the area occupied by the cytoplasm was 50 times greater than the Golgi apparatus. In addition, as indicated by the cytoplasm disintegration value (16 disintegrations compared with 43 actual grains), a majority of the actual grains which developed over the cytoplasm originated from a source other than the cytoplasm and thus resulted from the cross-fire of neighboring subcellular compartments. In contrast, the Golgi apparatus disintegration value (43 disintegrations compared with 15 actual grains)

TABLE 2. Relative specific activity of subcellular compartments in VZV-infected cells after pulse-chase labeling with [^{3}H]fucose

Subcellular compartment	Sp act for indicated chase period[a]							
	0 min	10 min	30 min	90 min	2 h	4 h	8 h	24 h
Cell membrane	1.30[b]	0.13	2.26	1.40	1.40	1.11	1.16	1.32
Cell membrane with virions[c]	0.00	0.00	0.00	0.00	0.00	18.87	12.93	14.32
Cytoplasm	1.14	0.77	0.53	0.67	−0.42	0.24	0.71	0.65
Golgi bodies	19.70	32.13	13.65	9.60	2.54	2.45	10.55	8.79
Post-Golgi region	1.63	−0.03	7.85	5.53	11.28	9.05	7.38	5.20
Cytoplasmic vacuoles	−0.37	0.98	0.59	5.58	22.27	6.95	4.69	3.82
Nucleus	0.17	0.26	0.03	0.12	0.43	0.07	0.07	0.12
Extracellular space	0.04	0.09	0.00	0.08	0.16	−0.04	0.04	−0.04

[a] All cultures were pulse labeled with [^{3}H]fucose for 30 min.

[b] Each relative specific activity value was calculated and normalized on an IBM XT desk-top computer so that subcellular compartments with significant radioactivities had values >1.

[c] Includes only cellular membrane areas associated with the egress of virions.

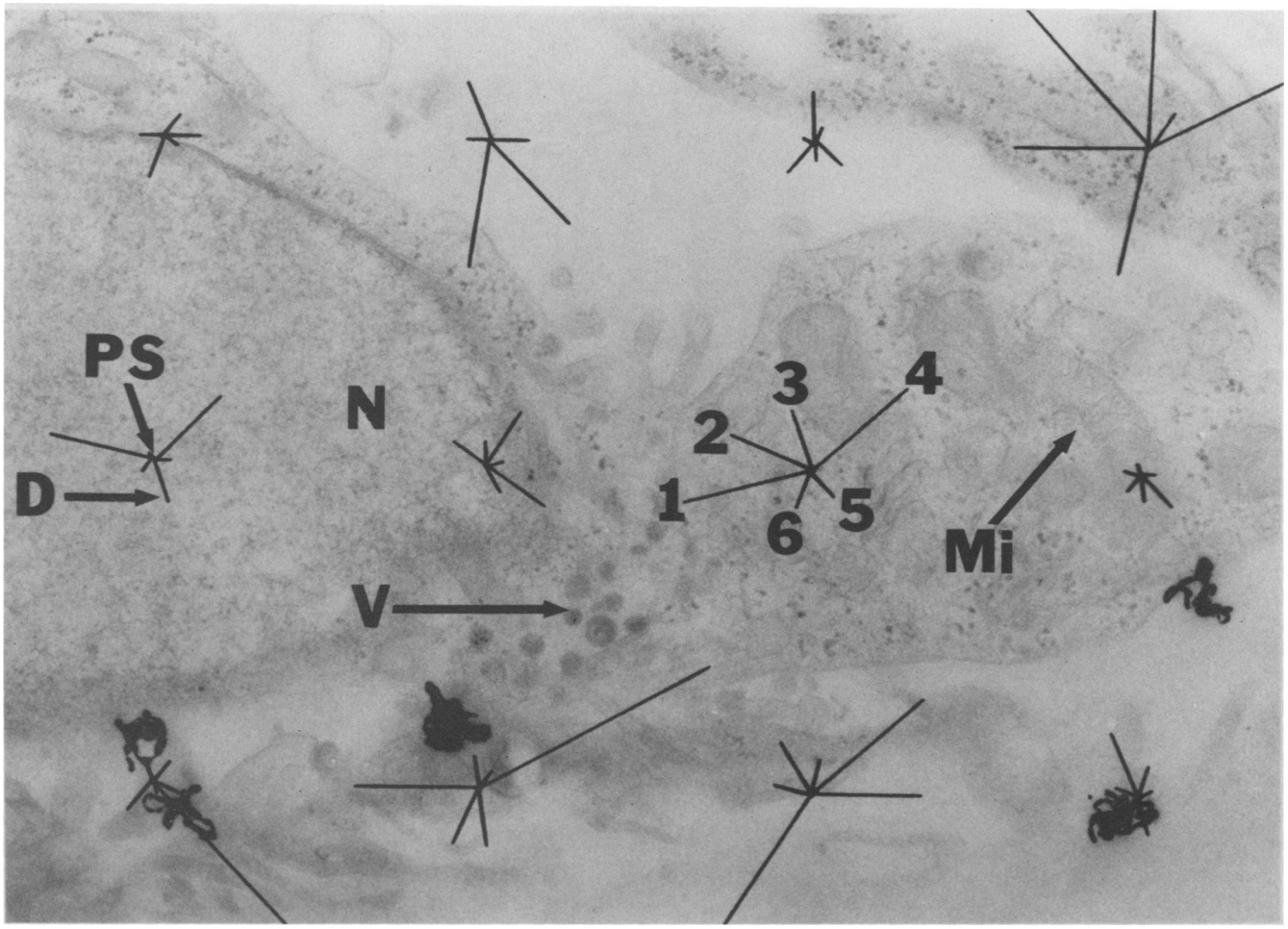

FIG. 4. Electron microscope autoradiography showing pulse-chase labeling with cross-fire correction overlay screen. VZV-infected HMC monolayers were pulse labeled with [^{3}H]fucose for 30 min and chased with label-free medium for 4 h. The monolayers were fixed and processed for electron microscope autoradiography as described in the text. The ARGs were printed at a final true magnification of ×18,750 on 8- by 10-in. (20.32- by 25.40-cm) paper. A cross-fire correction overlay screen was placed on top of the ARG, and the subcellular position of each hypothetical point source (PS) together with the subcellular position of six associated hypothetical disintegration points (D) was recorded in the CFPM. In this example, data derived from 12 point sources were accumulated for each micrograph analyzed. Finally, the subcellular positions of "real" silver grains were recorded. Abbreviations: N, nucleus; V, virions; Mi, mitochondria. Magnification, ×18,750.

indicated that a majority of the radioactive decays originating from within the Golgi apparatus produced silver grains within subcellular compartments other than the Golgi apparatus. When both cross-fire effect and area were considered, the final result showed a highly significant relative specific activity for [^{3}H]fucose (62.42) within the Golgi apparatus compared with an insignificant relative specific activity (0.43) within the cytoplasm (Table 1).

Subcellular trafficking of viral glycoproteins as determined by quantitative analysis after pulse-chase radiolabeling. The rationale for performing a pulse-chase quantitative analysis was twofold. First, we wished to determine whether cytoplasmic vacuoles were derived from the Golgi apparatus and post-Golgi vesicles. In addition, we wanted to investigate the role of cytoplasmic vacuoles in the envelopment and egress of VZV. After a 30-min pulse-labeling period with [^{3}H]fucose, VZV-infected monolayers were subjected to the following chase periods: 0, 10, 30, 90 min, and 2, 4, 8, and 24 h. Each time point was analyzed separately, and a detailed account of the relative specific activities obtained by CFPM analysis is presented in Table 2. An example of an electron microscope ARG with the cross-fire correction overlay screen is shown in Fig. 4. After a 30-min pulse of [^{3}H]fucose, the data indicated an accumulation of label within the Golgi apparatus which peaked after a 10-min chase period. Significant levels of labeling were also detected within the cellular membrane, cytoplasm, and post-Golgi region. However, the relative specific activity within these latter subcellular compartments decreased to insignificant levels after a 10-min chase period, thus suggesting the transport of radiolabel from these areas to the Golgi apparatus. After a 30-min chase period, the relative specific activity within the Golgi apparatus decreased, whereas the relative specific activity within the post-Golgi region increased to significant levels. Significant levels of radiolabel were first detected within the cytoplasmic vacuoles after a 90-min chase, and the relative specific activity increased dramatically after a 2-h chase. In addition, the relative specific activity within the Golgi apparatus and post-Golgi region decreased during the same chase period. Areas of the cellular membrane associated with the egress of mature enveloped virions accumulated significant levels of radiolabel after a 4-h chase. This result was

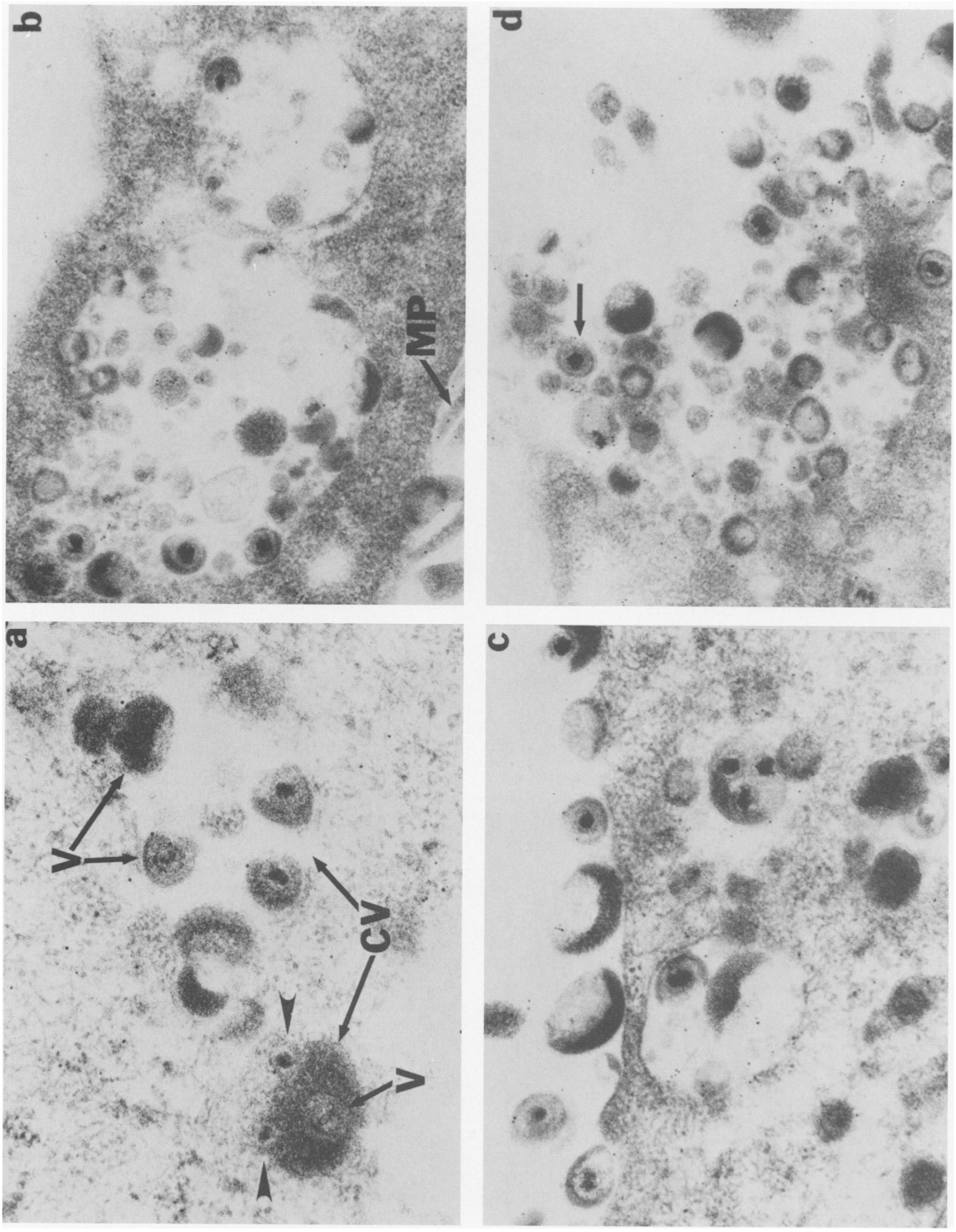
b
MP
d
a
V
CV
V
c

accompanied by a substantial decrease in relative specific activity within the cytoplasmic vacuoles. Therefore, the data taken together after a 4-h chase period suggested a movement or flow of [^{3}H]fucose from the Golgi apparatus through the post-Golgi region into cytoplasmic vacuoles; the vacuoles in turn migrated and fused with the cellular membrane, with a resultant release of enveloped virions. Label within regions of the cellular membrane not associated with enveloped virions maintained a low level of activity throughout the experiment. As shown previously in the continuous labeling experiments, insignificant levels of radiolabel were reported within the cytoplasm (excluding the 0-min pulse), nucleus (including the nuclear membrane), and extracellular space.

Immunocytochemical localization of VZV glycoproteins. Monoclonal antibody 3B3 specifically recognizes VZV gpI, which is the predominant glycoprotein species inserted into the membranes of VZV-infected cells (11, 45). This antibody was used to stain Lowicryl K4M-embedded VZV-infected HMC monolayers, and bound antibody was localized with goat anti-mouse immunoglobulin G conjugated with 10-nm gold particles. Specific gpI localization was observed within cytoplasmic vacuoles, on mature enveloped virions, and on microvillus projections at the cellular membrane (Fig. 5).

Thin sections of Lowicryl K4M-embedded VZV-infected monolayers revealed several morphological forms of virion envelope and cytoplasmic vacuole membranes, each varying in their degree of gold labeling. Enveloped virions and cytoplasmic vacuoles were commonly observed partially or completely enclosed within a homogeneous dense material which was not immunoreactive. These virions and cytoplasmic vacuoles which were covered within a thickened electron-dense region bound few gold particles in this area (Fig. 5a); however, vacuoles sectioned to expose their interiors contained several gold particles localized on enveloped virions and vacuole membranes (Fig. 5b and c). In addition, gpI localization on enveloped virions was most commonly observed at the outermost limiting envelope. This globular structured fringe may represent gpI spike projections from the viral envelope, which are most clearly illustrated in Fig. 5d. Similar spike projections were shown by high-resolution electron microscope immunochemistry to bind antibodies specific for three major glycoproteins of HSV type 1 (40).

DISCUSSION

The VZV genome encodes several glycoproteins which are present within both mature viral envelopes and the cellular membrane of infected cells. However, the mechanism of intracellular glycoprotein transport and the site at which nucleocapsids acquire their glycoprotein envelope have not been well defined. It the present study, we utilized electron microscope autoradiography with [^{3}H]fucose continuous and pulse-chase labeling to elucidate the role of cytoplasmic vacuoles in VZV envelopment and the trafficking of viral glycoproteins. An inherent problem when assessing the silver grain distribution of an electron microscope ARG is that silver grains from one radioactive source may overlay a subcellular compartment other than that wherein the radioactive decay originated. This anomaly is termed cross-fire and is never insignificant when assessing electron microscope autoradiographic experiments (9). Should several subcellular compartments be radioactive and each vary with respect to shape, size, and spatial arrangement, the pattern of cross-fire and thus silver grain distribution would be extremely complex and not amenable to simple quantitative analysis. By ignoring the efficacy of cross-fire, one may greatly underestimate the activity within relatively small radioactive sources and overestimate the activity in relatively large radioactive sources (48). The CFPM analysis method used in this study takes into account the cross-fire which occurs among neighboring subcellular compartments. Therefore, we were able to obtain an accurate estimate of the specific activity within each subcellular compartment (5).

One route of VZV glycoprotein trafficking through infected cells was clearly demonstrated by analysis of the

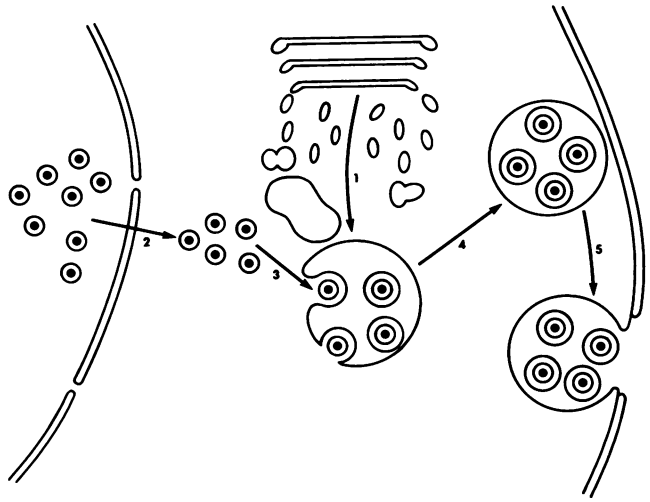

FIG. 6. Schema for trafficking of VZV glycoproteins and egress of enveloped VZV particles. Glycoproteins processed in the Golgi apparatus are released at the trans-Golgi within small transport vesicles. Fusion of these vesicles at the post-Golgi region results in the formation of large glycoprotein-laden cytoplasmic vacuoles (arrow 1). Naked nucleocapsids released in the perinuclear space (arrow 2) migrate and bud into the cytoplasmic vacuoles (arrow 3). Enveloped virions are transported to the cellular membrane within the cytoplasmic vacuoles (arrow 4) and are subsequently released upon fusion of the limiting membrane of the vacuole with the cellular membrane (arrow 5). This schema incorporates some features previously described for HSV by Rodriguez and Dubois-Dalcq (34).

FIG. 5. Immunodetection of VZV glycoproteins at sites of viral envelopment and egress. Infected HMC monolayers were fixed in 5% paraformaldehyde and embedded in Lowicryl K4M. Thin sections were immunolabeled with anti-VZV gpI monoclonal antibody, and bound primary antibody was detected with goat anti-mouse antibody conjugated with 10-nm gold particles. Specific gpI localization was observed within cytoplasmic vacuoles (CV), enveloped virions (V), and microvillus projections (MP) at the cellular membrane. However, few gold particles were observed bound to the thickened electron-dense material present on some cytoplasmic vacuoles and virions. In addition, gold particles bound to virions were most commonly observed at the outermost limiting envelope (arrow in panel d). This figure also illustrates a possible sequence of viral egress from infected cells. Two naked nucleocapsids are observed entering a cytoplasmic vacuole in panel a (arrowheads). Vacuoles harboring enveloped virions migrated to localized regions of the cellular membrane (panels b and c) in which fusion with the cellular membrane occurred, with a concomitant release of mature enveloped virions (panel d). Magnification of panels, ×66,750, ×44,500, ×55,625, ×44,500, respectively.

[^{3}H]fucose pulse-chase experiments. Fucose, being a terminal sugar, is incorporated into immature glycoproteins exclusively within the Golgi apparatus (21). The quantitative results obtained from these studies support the hypothesis for VZV envelopment and egress illustrated in Fig. 6. This schema includes the following points. Mature glycoproteins exit the trans-Golgi cisternae within membranes of post-Golgi transport vesicles. Fusion of these glycoprotein-laden carrier vesicles, possibly mediated by the presence of viral glycoproteins (28), leads to the formation of large virus-induced cytoplasmic vacuoles bound by one or more limiting membranes. Naked nucleocapsids, released from the nucleus, bud through the cytoplasmic vacuole membrane and thereby obtain their glycoprotein-rich envelope. Transportation of the mature enveloped virions to the cellular membrane occurs via the cytoplasmic vacuoles, and exit of virions at the cellular membrane takes place when cytoplasmic vacuoles harboring VZV particles fuse and become incorporated into the cellular membrane.

Similar studies of [^{3}H]fucose kinetics and pathways have been carried out in a variety of mammalian cell types, including both secretory and nonsecretory as well as static and expanding cells (3, 41). These investigations included over 50 different cell types, which were examined by both light and electron microscope autoradiography techniques. The authors conclude that the mature glycoproteins migrate from the Golgi apparatus to the cellular membrane in Golgi-derived carrier vesicles. After being processed in the Golgi apparatus, the glycoproteins passed into either coated carrier vesicles of 70 to 120 nm or, more commonly, into smooth-surfaced carrier vesicles which varied in size from 100 to 300 nm (23). Thus, these carrier vesicles are considerably smaller than the cytoplasmic vacuoles associated with the envelopment and transport of VZV particles. The latter vacuoles typically were larger than 500 nm in diameter; indeed, some were 3.5 μm and transversed the entire cell width.

The cytoplasmic transport of VZV glycoproteins may occur by a bulk-flow mechanism from the trans-Golgi cisternae. According to the bulk-flow transport hypothesis, proteins not retained within the endoplasmic reticulum or the Golgi membranes migrate through the Golgi cisternae by default and concentrate at regions in which vesicles could form, such as the rims of Golgi stacks (31). Vesicles which form in these regions have a coat other than clathrin and mediate the biosynthetic transport of proteins within the Golgi apparatus by budding from one set of cisternae and fusing with the next (30). In contrast, the transport of proteins within clathrin-coated vesicles occurs via a selective signal-mediated pathway (31). Although vesicular stomatitis virus G protein has been isolated from clathrin-coated vesicles (37), Orci et al. (30) have recently suggested that the transport of this viral glycoprotein occurs primarily via a nonselective bulk-flow transport mechanism. Bulk-flow transport of membrane proteins from the Golgi apparatus to the cellular membrane is blocked by the ionophore monensin. Therefore, proteins transported to the cellular membrane by a nonselective constituitive pathway are to be inhibited by monensin (22, 42–44). Evidence indicating that monensin completely inhibits VZV and vesicular stomatitis virus glycoprotein transport (1, 14, 24), but not that of influenza virus (1), suggests that VZV and vesicular stomatitis virus utilize a similar bulk-flow glycoprotein transport mechanism.

Other researchers have suggested that the primary site of HSV type 1 envelopment is the inner nuclear membrane (15, 32, 39). Envelopment at the nuclear membrane may require an additional processing step because only core high-mannose glycoproteins appear to be present within the nuclear envelope (6). One hypothesis suggests that enveloped HSV virions from the perinuclear cisterna obtain their terminal processed sugars by physically migrating through the Golgi apparatus (16, 32, 39). An alternative schema for virus envelopment which includes cytoplasmic vacuoles as the primary site of HSV envelopment late in infection was proposed earlier by Rodriguez and Dubois-Dalcq (34) and, to a lesser extent, by Nii (27). In the latter studies, cytoplasmic vacuoles were shown to possess the same globular molecular membrane structure and intramembrane particle density as enveloped virions and particles in the extracellular space (27, 34). In contrast, the envelopes of virions found in the nucleus and at the perinuclear cisternae have a lower intramembrane particle density and lack a globular membrane structure (27, 34). The high intramembrane particle density observed on cytoplasmic vacuoles and enveloped virions within the extracellular space may represent an organization of membrane protein exclusive of viral origin (34). These observations support our data which showed a high [^{3}H]fucose specific activity representing mature viral glycoproteins within cytoplasmic vacuoles but not within the nucleus. In conclusion, the envelopment of herpesviruses may occur by two mechanisms which are not necessarily mutually exclusive. In this communication, we have presented evidence suggesting that the major site of VZV envelopment is within virally induced cytoplasmic vacuoles rather than the nuclear membrane.

ACKNOWLEDGMENTS

We thank M. F. Stinski for his critical review.

This research was supported by Public Health Service grant AI22795 from the National Institute of Allergy and Infectious Diseases and by grant MV-359 from the American Cancer Society.

LITERATURE CITED

1. **Alonso, F. V., and R. W. Compans.** 1981. Differential effect of monensin on enveloped viruses that form at distinct plasma membrane domains. J. Cell Biol. **89**:700–705.
2. **Atkinson, M. A., S. Barr, and M. C. Timbury.** 1978. The fine structure of cells infected with temperature-sensitive mutants of herpes simplex virus type 2. J. Gen. Virol. **40**:103–119.
3. **Bennett, G., C. P. Leblond, and A. Haddad.** 1974. Migration of glycoprotein from the Golgi apparatus to the surface of various cell types as shown by radioautography after labeled fucose injection into rats. J. Cell Biol. **60**:258–284.
4. **Blackett, N. M., and D. M. Parry.** 1973. A new method for analyzing electron microscope autoradiographs using hypothetical grain distributions. J. Cell Biol. **57**:9–15.
5. **Blackett, N. M., and D. M. Parry.** 1977. A simplified method of "hypothetical grain" analysis of electron microscope autoradiographs. J. Histochem. Cytochem. **25**:206–214.
6. **Compton, T., and R. J. Courtney.** 1984. Virus-specific glycoproteins associated with the nuclear fraction of herpes simplex virus type 1-infected cells. J. Virol. **49**:594–597.
7. **Cook, M. L., and J. G. Stevens.** 1970. Replication of varicella-zoster virus in cell culture: an ultrastructural study. J. Ultrastruct. Res. **32**:334–350.
8. **Dargan, D. J.** 1986. The structure and assembly of herpesviruses, p. 359–437. *In* J. R. Harris and R. W. Horne (ed.), Electron microscopy of proteins, vol. 5. Viral structure. Academic Press, Inc., New York.
9. **Downs, A., and M. A. Williams.** 1978. An iterative approach to the analysis of electron microscope autoradiographs. I. The method. J. Microsc. (Oxford) **114**:143–156.
10. **Grose, C.** 1980. The synthesis of glycoproteins in human melanoma cells infected with varicella-zoster virus. Virology **101**:1–

9.
11. **Grose, C.** 1987. Varicella zoster virus: pathogenesis of the human diseases, the virus and viral replication, and the major viral glycoproteins and proteins, p. 1–65. *In* R. W. Hyman (ed.), Natural history of varicella-zoster virus. CRC Press, Boca Raton, Fla.
12. **Grose, C., D. M. Perrotta, P. A. Brunell, and G. C. Smith.** 1979. Cell-free varicella-zoster virus in cultured human melanoma cells. J. Gen. Virol. **43**:15–27.
13. **Heine, U., D. V. Ablashi, and G. R. Armstrong.** 1971. Morphological studies on herpesvirus saimiri in subhuman and human cell cultures. Cancer Res. **31**:1019–1029.
14. **Johnson, D. C., and M. J. Schlesinger.** 1980. Vesicular stomatitis virus and sindbis virus glycoprotein transport to the cell surface is inhibited by ionophores. Virology **103**:407–424.
15. **Johnson, D. C., and P. G. Spear.** 1982. Monensin inhibits the processing of herpes simplex virus glycoproteins, their transport to the cell surface, and the egress of virions from infected cells. J. Virol. **43**:1102–1112.
16. **Johnson, D. C., and P. G. Spear.** 1983. O-linked oligosaccharides are acquired by herpes simplex virus glycoproteins in the Golgi apparatus. Cell **32**:987–997.
17. **Karnovsky, M. J.** 1965. A formaldehyde-gluteraldehyde fixative of high osmolality for use in electron microscopy. J. Cell Biol. **27**:137.
18. **Karnovsky, M. J.** 1971. Use of ferrocyanide reduced osmium tetraoxide in electron microscopy. J. Cell Biol. **51**:146.
19. **Katsumoto, T., A. Hirano, T. Kurimura, and A. Takagi.** 1981. In situ electron microscopical observation of cells infected with herpes simplex virus. J. Gen. Virol. **52**:267–278.
20. **Kopriwa, B. M.** 1975. A comparison of various procedures for fine grain development in electron microscopic radioautography. Histochemistry **44**:201–224.
21. **Kornfeld, R., and S. Kornfeld.** 1985. Assembly of asparagine-linked oligosaccharides. Annu. Rev. Biochem. **54**:631–664.
22. **Ledger, P. W., N. Uchida, and M. L. Tanzer.** 1980. Immunocytochemical localization of procollagen and fibronectin in human fibroblasts: effects of the monovalent ionophore, monensin. J. Cell Biol. **87**:663–671.
23. **Michaels, J. E., and C. P. Leblond.** 1976. Transport of glycoprotein from Golgi apparatus to cell surface by means of "carrier" vesicles, as shown by radioautography of mouse colonic epithelium after injection of ^{3}H-fucose. J. Microsc. Biol. Cell. **25**:243–248.
24. **Montalvo, E. A., R. T. Parmley, and C. Grose.** 1985. Structural analysis of the varicella-zoster virus gp98-gp62 complex: post-translational addition of N-linked and O-linked oligosaccharide moieties. J. Virol. **53**:761–770.
25. **Montalvo, E. A., R. T. Parmley, and C. Grose.** 1986. Varicella-zoster viral glycoprotein envelopment: ultrastructural cytochemical localization. J. Histochem. Cytochem. **34**:281–284.
26. **Nii, S.** 1971. Electron microscopic observations on FL cells infected with herpes simplex virus. I. Viral forms. Biken J. **14**: 177–190.
27. **Nii, S.** 1971. Electron microscopic observations on FL cells infected with herpes simplex virus. II. Envelopment. Biken J. **14**:325–348.
28. **Nii, S., C. Morgan, H. M. Rose, and K. C. Hsu.** 1968. Electron microscopy of herpes simplex virus. IV. Studies with ferritin-conjugated antibodies. J. Virol. **2**:1172–1184.
29. **O'Callaghan, D. J., and C. C. Randall.** 1976. Molecular anatomy of herpesviruses: recent studies. Prog. Med. Virol. **22**:152–210.
30. **Orci, L., B. S. Glick, and J. E. Rothman.** 1986. A new type of coated vesicular carrier that appears not to contain clathrin: its possible role in protein transport within the Golgi stack. Cell **46**: 171–184.
31. **Pfeffer, S. R., and J. E. Rothman.** 1987. Biosynthetic protein transport and sorting by the endoplasmic reticulum and Golgi. Annu. Rev. Biochem. **56**:829–852.
32. **Poliquin, L., G. Levine, and G. C. Shore.** 1985. Involvement of the Golgi apparatus and a restructured nuclear envelope during biogenesis and transport of herpes simplex virus glycoproteins. J. Histochem. Cytochem. **33**:875–883.
33. **Reynolds, E. S.** 1963. The use of lead citrate at high pH as an electron-opaque stain in electron microscopy. J. Cell Biol. **17**: 208–213.
34. **Rodriguez, M., and M. Dubois-Dalcq.** 1978. Intramembrane changes occurring during maturation of herpes simplex virus type 1: freeze-fracture study. J. Virol. **26**:435–447.
35. **Rogers, A. W.** 1979. Techniques of autoradiography, p. 133–200. Elsevier Biomedical Press, Amsterdam.
36. **Roth, J., M. Bendayan, E. Carlemalm, W. Villiger, and M. Garavito.** 1981. Enhancement of structural preservation and immunocytochemical staining in low temperature embedded pancreatic tissue. J. Histochem. Cytochem. **29**:663–671.
37. **Rothman, J. E., and R. E. Fine.** 1980. Coated vesicles transport newly synthesized membrane glycoproteins from endoplasmic reticulum to plasma membrane in two successive stages. Proc. Natl. Acad. Sci. USA **77**:780–784.
38. **Salpeter, M. M., L. Bachmann, and E. E. Salpeter.** 1969. Resolution in electron microscope radioautography. J. Cell Biol. **41**:1–20.
39. **Spear, P. G.** 1985. Glycoproteins specified by herpes simplex virus, p. 315–356. *In* B. Roizman (ed.), The herpesviruses, vol. 3. Plenum Publishing Corp., New York.
40. **Stannard, L. M., A. O. Fuller, and P. G. Spear.** 1987. Herpes simplex virus glycoproteins associated with different morphological entities projecting from the virion envelope. J. Gen. Virol. **68**:715–725.
41. **Sturgess, J. M., E. Minaker, M. M. Mitranic, and M. A. Moscarello.** 1973. The incorporation of L-fucose into glycoproteins in the Golgi apparatus of rat liver and in serum. Biochim. Biophys. Acta **320**:123–132.
42. **Tartakoff, A., and P. Vassalli.** 1978. Comparative studies of intracellular transport of secretory proteins. J. Cell Biol. **79**: 694–707.
43. **Tartakoff, A. M., and P. Vassalli.** 1977. Plasma cell immunoglobulin in secretion: arrest is accompanied by alterations of the Golgi complex. J. Exp. Med. **146**:1332–1345.
44. **Uchida, N., H. Smilowitz, and M. L. Tanzer.** 1979. Monovalent ionophores inhibit secretion of procollagen and fibronectin from cultured human fibroblasts. Proc. Natl. Acad. Sci. USA **76**: 1868–1872.
45. **Weigle, K. A., and C. Grose.** 1983. Common expression of varicella-zoster viral glycoprotein antigens in vitro and in chickenpox and zoster vesicles. J. Infect. Dis. **148**:630–638.
46. **Williams, M. A.** 1969. The assessment of electron microscopic autoradiographs, p. 219–272. *In* R. Barer and V. E. Cosslett (ed.), Advances in optical and electron microscopy, vol. 3. Academic Press, Inc., New York.
47. **Williams, M. A.** 1977. Autoradiography and immunochemistry, p. 77–163. *In* A. Glavert (ed.), Practical methods of electron microscopy, vol. 6, pt. 1. Elsevier Biomedical Press, Amsterdam.
48. **Williams, M. A.** 1982. Autoradiography: its methodology at the present time. J. Microsc. **128**:79–94.
49. **Williams, M. A., and A. Downs.** 1978. An iterative approach to the analysis of electron microscope autoradiographs. II. Estimates of sample sizes and confidence limits. J. Microsc. **114**: 157–178.